Supplementary material

The supplementary material for the J. Appl. Cryst. publication "Determining grain resolved stresses in polycrystalline materials using 3DXRD" by J. Oddershede *et al.* comprises plots of the evolution in the average non-axial strain components and applied stresses of the 96 IF steel grains during the elastic loading and unloading (Figures 1–5). These plots correspond to the average stress/strain curve, Figure 5 in the publication.

Furthermore Figures 6–11 display the evolution in the derived average stress tensor components as a function of the applied stress. While the strain averages are simple averages, the stress averages are volume weighted and the values have been corrected for the 130×10^{-6} zero point off-set in ϵ_{22} (Figure 2).

For all figures the applied stresses and error bars are obtained from the load cell readings, while the error bars on the average strains and stresses are propagated from the corresponding estimated errors on the grain resolved properties.

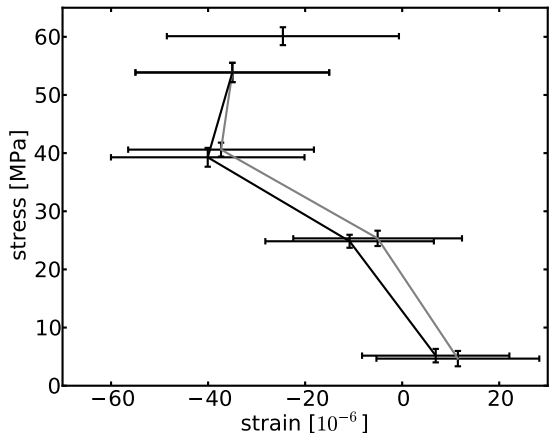

Figure 1: The evolution in the average normal strain component ϵ_{11} (perpendicular to the incoming beam at $\omega = \pm 90°$) and the applied stress during the elastic loading (grey) and unloading (black).

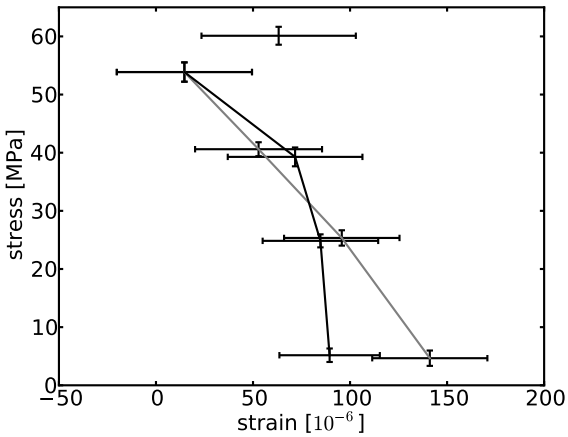

Figure 2: The evolution in the average normal strain component ϵ_{22} (parallel to the incoming beam at $\omega = \pm 90°$ – the direction geometrically least favourable) and the applied stress during the elastic loading (grey) and unloading (black). Note the zero-point off-set of 130×10^{-6}.

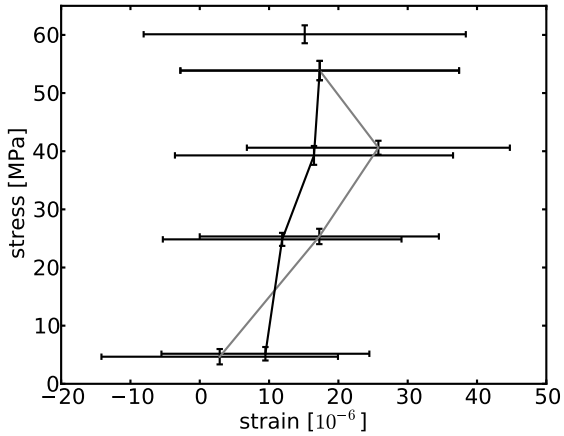

Figure 3: The evolution in the average shear strain component ϵ_{12} (in the plane perpendicular to the tensile axis) and the applied stress during the elastic loading (grey) and unloading (black).

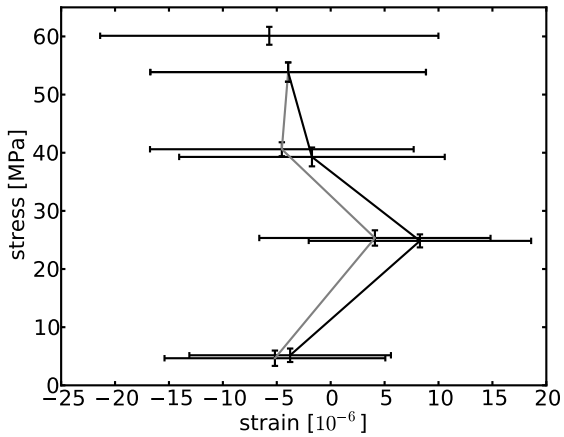

Figure 4: The evolution in the average shear strain component ϵ_{13} (in the plane perpendicular to the incoming beam at $\omega = \pm 90°$) and the applied stress during the elastic loading (grey) and unloading (black).

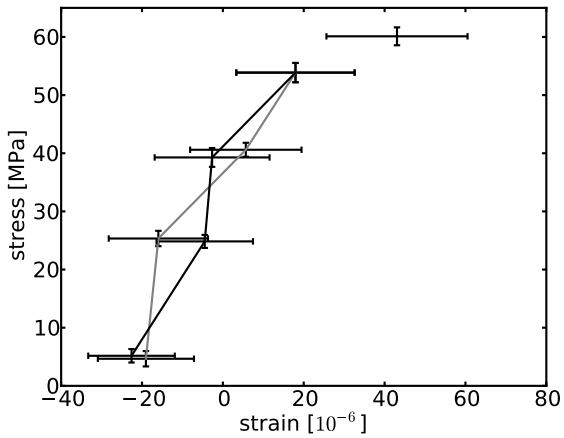

Figure 5: The evolution in the average shear strain component ϵ_{23} (in the plane perpendicular to the incoming beam at $\omega = 0°$) and the applied stress during the elastic loading (grey) and unloading (black).

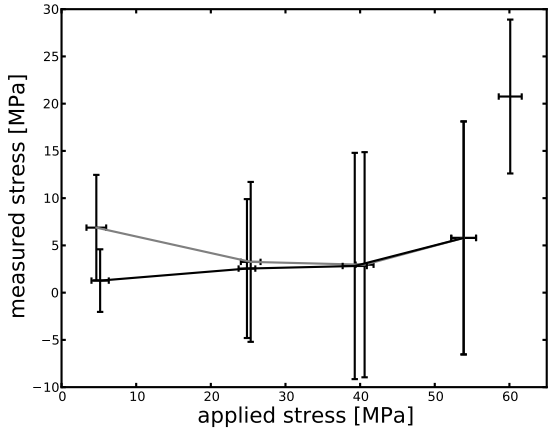

Figure 6: The evolution in the average normal stress component σ_{11} (perpendicular to the incoming beam at $\omega = \pm 90°$) as a function of applied stress during the elastic loading (grey) and unloading (black).

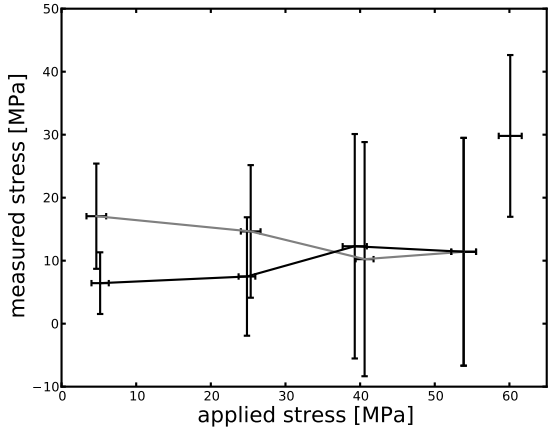

Figure 7: The evolution in the average normal stress component σ_{22} (parallel to the incoming beam at $\omega = \pm 90°$ – the direction geometrically least favourable) as a function of applied stress during the elastic loading (grey) and unloading (black).

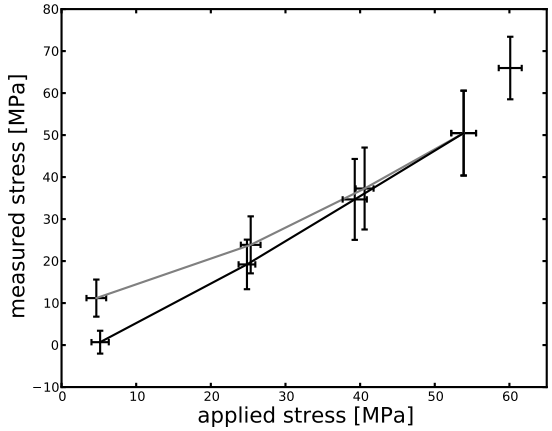

Figure 8: The evolution in the average axial stress component σ_{33} as a function of applied stress during the elastic loading (grey) and unloading (black).

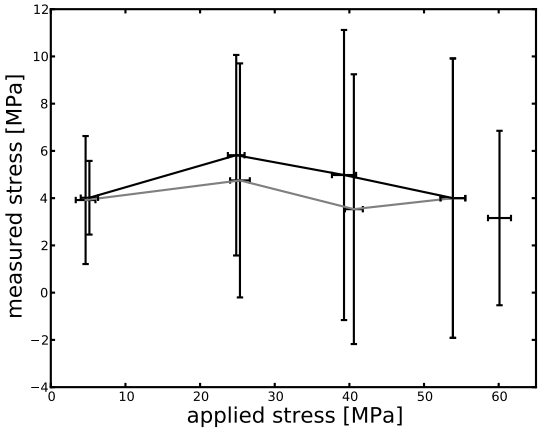

Figure 9: The evolution in the average shear stress component σ_{12} (in the plane perpendicular to the tensile axis) as a function of applied stress during the elastic loading (grey) and unloading (black).

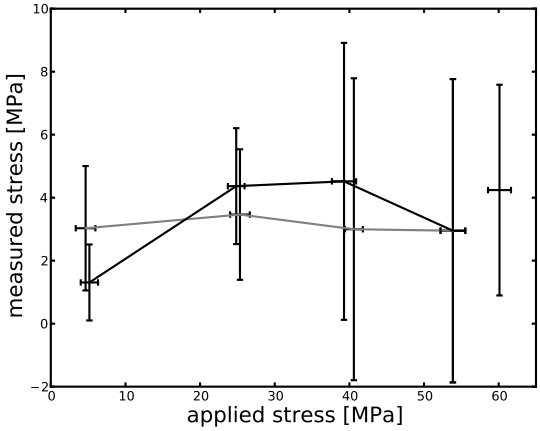

Figure 10: The evolution in the average shear stress component σ_{13} (in the plane perpendicular to the incoming beam at $\omega = \pm 90°$) as a function of applied stress during the elastic loading (grey) and unloading (black).

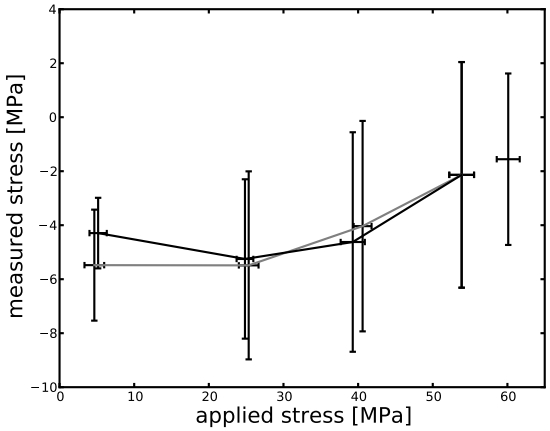

Figure 11: The evolution in the average shear stress component σ_{23} (in the plane perpendicular to the incoming beam at $\omega = 0°$) as a function of applied stress during the elastic loading (grey) and unloading (black).